Electronic Supplementary Material (ESI) for Soft Matter.

Supplementary Information

Clostridium perfringens α-toxin interaction with red cells and model membranes

S. A. Jewell, R. W. Titball, J. Huyet, C. E. Naylor, A. K. Basak, P. Gologan, C. P. Winlove, P. G. Petrov

Accumulation of products of hydrolysis in red cell membranes

Accumulation of products of hydrolysis in droplets embedded in the membrane is also observed in red blood cells exposed to α-toxin. Figure S1 shows two snapshots of a cell population 10 minutes (A) and 30 minutes (B) after the addition of the toxin. Before addition of toxin, the majority of the cells in this sample were discocytic. Axisymmetric and non-axisymmetric stomatocytes are the dominant shapes after the sample has been exposed to toxin for 10 minutes (Figure S1A). Further hydrolysing activity leads to formation of bright droplets of hydrolysis products embedded in the membrane (Figure S1B) similarly to lipid vesicles.

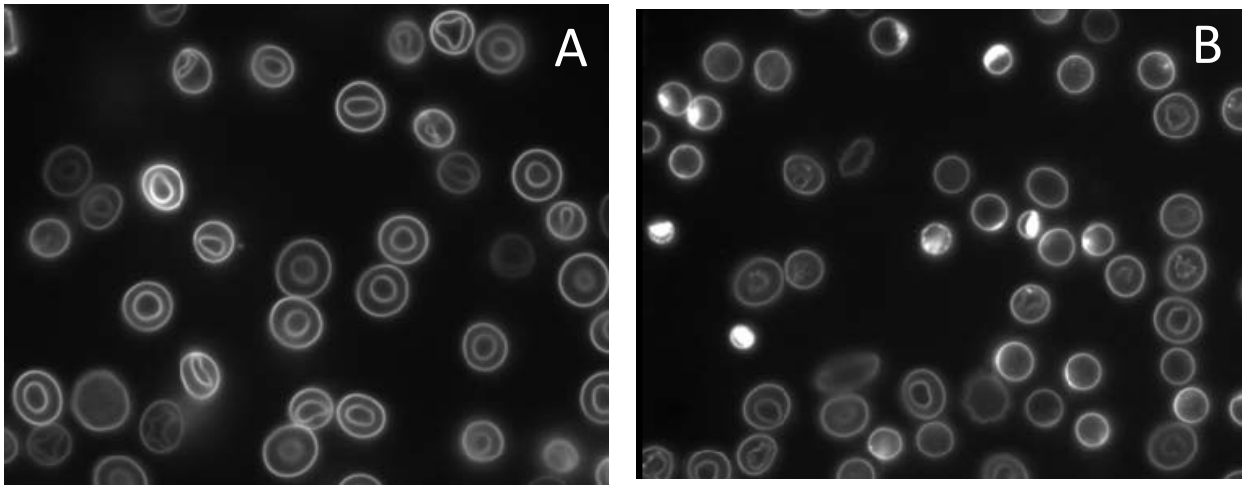

Figure S1. Fluorescence microscopy images of Di-8-ANEPPS labelled red blood cells 10 min (A) and 30 min (B) after the addition of α-toxin. Toxin concentration 1.4 nM. The fluorescence images are obtained using an excitation wavelength of 420 nm and emission wavelength of 650 nm.

Effect of α-toxin on red cell morphology

Interaction between α-toxin and red blood cell can result in (i) changes in cell morphology and (ii) partial or full haemolysis. Cells respond to toxin in a concentration-dependent manner. At high concentrations, morphological changes are accompanied by partial or full loss of haemoglobin by the cell (see Figures 9 and 10 in the main paper, where the toxin concentration was 1.4 nM). At low concentration, the toxin is able to elicit morphological changes but not necessarily lyse the cell. Figure S2 shows the morphological response of a cell incubated with 0.18 nM α-toxin. This figure, along with the analysis of the radial distribution of the optical density (Figure S3) demonstrate a considerable transformation in cell shape. However, the integrated optical density, a measure for the cell haemoglobin content, remains constant (Figure S4) despite the changes in cell radius and morphology. This response is different from that at high toxin concentration, where haemolysis is observed (Figure 10B in the main paper) along with changes in cell shape.

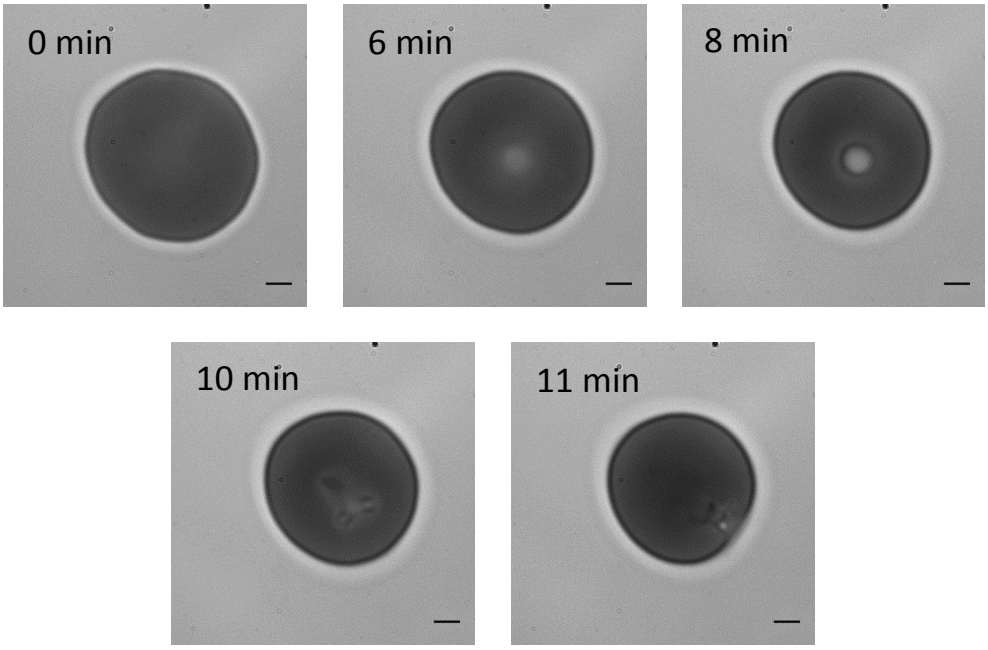

Figure S2. Microscopy images illustrating morphological changes in a red blood cell as a result of α-toxin activity. The images are obtained using transmission microscopy at 415 nm. The scale bar indicates 1 μm. Toxin concentration 0.18 nM.

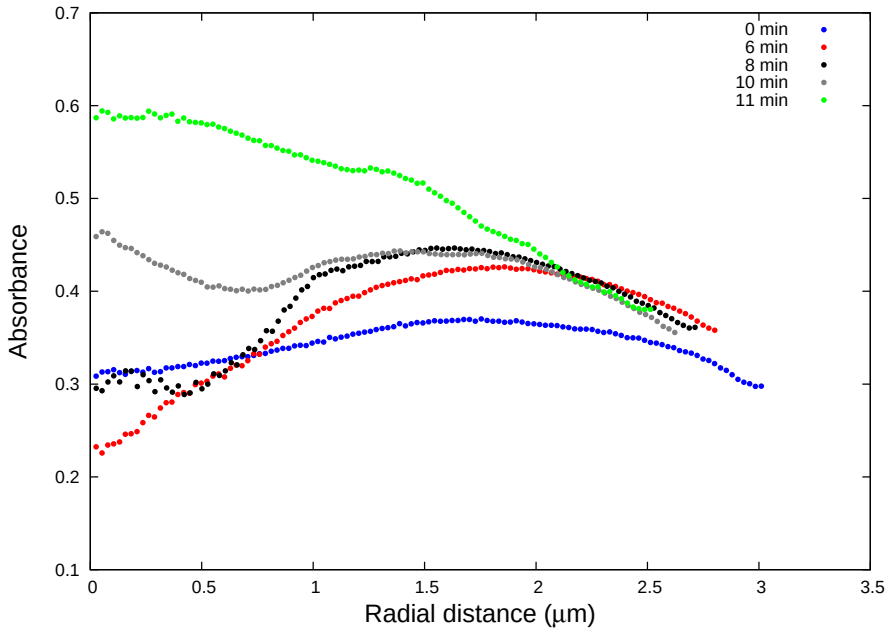

Figure S3. Variations of the absorbance of 415 nm light with radius indicating the relative change in thickness for the cell shown in Figure S2. Toxin concentration 0.18 nM.

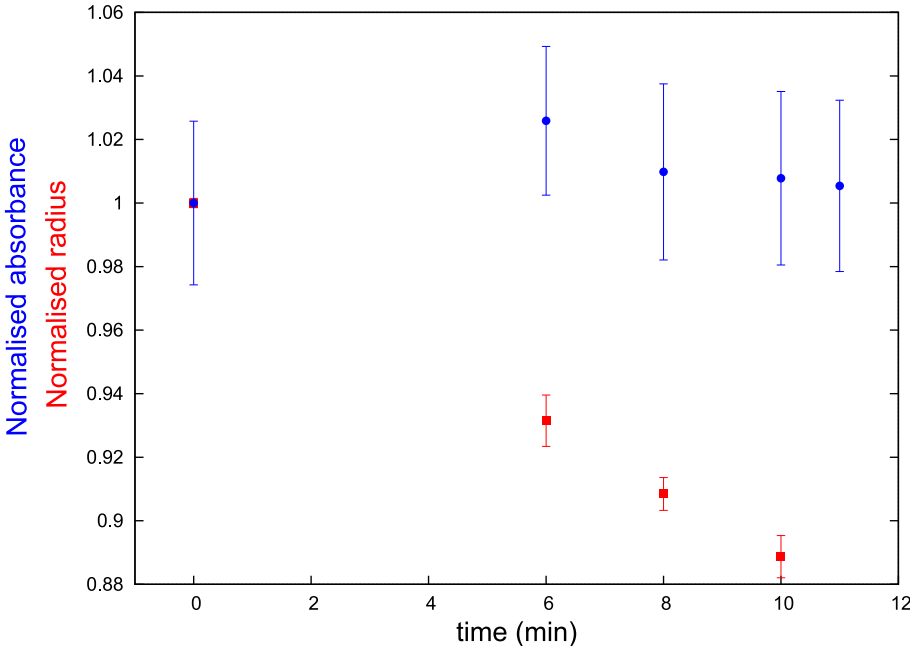

Figure S4. Changes of the mean cell radius (red squares) and integrated optical density (blue circles) for the cell shown in Figure S2. The values for the radius and the optical density are normalised to the corresponding values before addition of toxin (i.e. 0 min). Toxin concentration 0.18 nM.

For comparison Figure S5 shows an example of the haemolytic activity of a different type of toxin, NetB. NetB is a β-pore-forming toxin produced by *Clostridium perfringens*[1] known to induce cell lysis[2]. As can be seen in Figure S5, at this particular concentration the cell radius and haemoglobin content remain constant in the first 20 minutes after the addition of toxin. The onset of haemolysis is clearly identifiable by the sudden drop in the integrated optical density at t = 20 min, an event that also coincides with the change in mean cell radius.

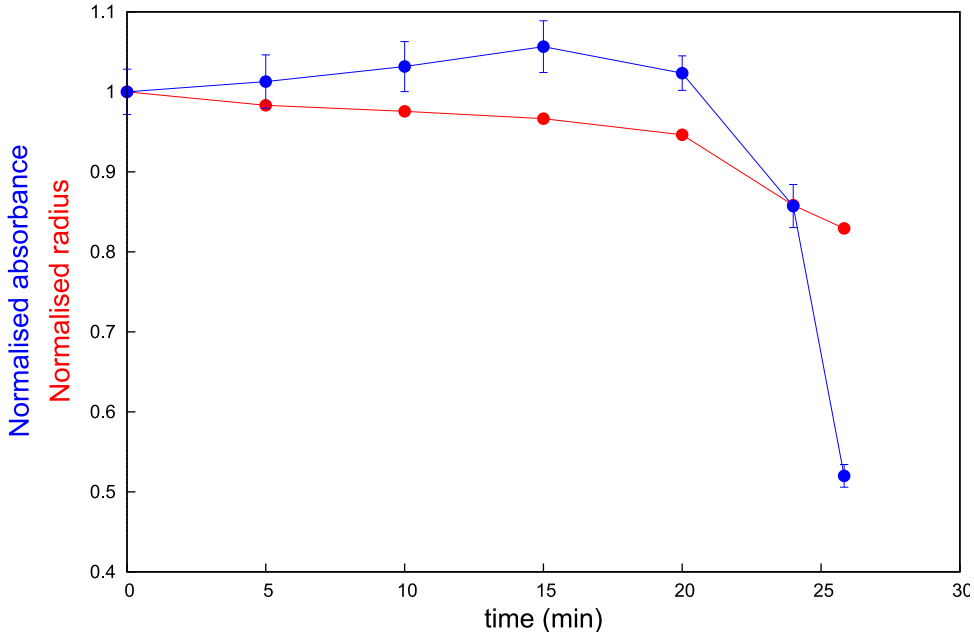

Figure S5. Changes of the mean cell radius (red squares) and integrated optical density (blue circles) for a cell exposed to the pore-forming toxin NetB. The values for the radius and the optical density are normalised to the corresponding values before addition of toxin (i.e. 0 min). Toxin concentration 28 nM.

Analysis of mean cell shapes

The effects on cell shapes at low toxin concentrations reported in Section 3.4.3 of the main paper are small. Here we present justification for the methodology used and show how a red blood cell could be used as a reporter for cell-solute interactions[3]. We carried out a separate set of experiments in which the shapes of red cells were manipulated in a controlled fashion, and investigated the cell morphological response through the contour Fourier representation (Equation 1 in the main paper). As explained in the main paper, upon a transition between a discocyte and an echinocyte, we expect to see changes in the mean value of the 9th Fourier amplitude, since the first echinocytic shape to emerge from this transition is E1-9, a flat echinocyte with 9 undulations around the equatorial contour[4].

In the first experiment, we induced a transition from a discocyte to an echinocyte by exchanging the buffer solution around the cell with a buffer containing 8 mM sodium salicylate, a known echinocytogenic substance[5]. Subsequently, the buffer around the cell was exchanged with one containing 10 μM of chlorpromazine, a compound known to promote the formation of stomatocytes[6]. The results of such an experiment are summarised in Figure S6, along with a representation of the instantaneous and mean values of c_9. Upon addition of sodium salicylate, the initial discocyte transforms into an echinocyte. This transition is clearly detected by an increase in $\langle c_9 \rangle$ as expected from theory. Chlorpromazine reverses this transition driving the cell through a discocytic shape into a stomatocyte. In this case we observe a decrease in $\langle c_9 \rangle$, since the equatorial contour of the stomatocyte (Figure S6) is more circular than that of the echinocyte.

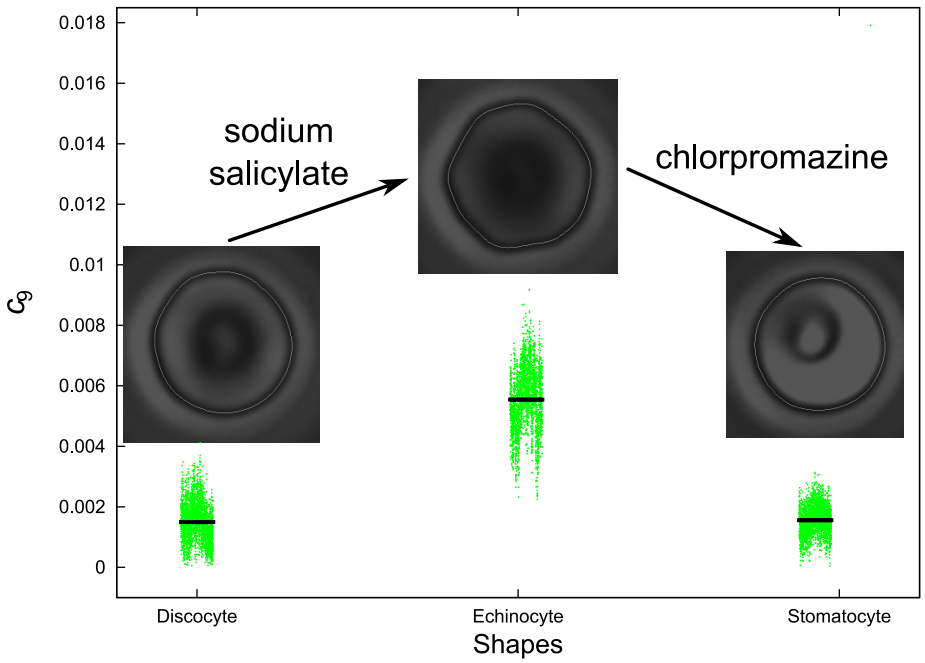

Figure S6. Changes in the 9th Fourier mode amplitude as a result of shape transitions induced by sodium salicylate and chlorpromazine. The points in each green cluster represent the instantaneous values of c_9. The black line across each cluster is the mean value for this amplitude, $\langle c_9 \rangle$. Representative snapshots (phase contrast) of the corresponding shapes are shown above each cluster. The white line is the reconstructed contour.

In the second control experiment, we induced a shape transition using a different method. Cells were suspended in a solution containing 137 mM NaCl and 2 mM potassium ferrocyanide ($K_4[Fe(CN)_6 \cdot 3H_2O$, Sigma-Aldrich, UK). The pH of the solution was adjusted to 7.4 by addition of either NaOH or HCl before suspending the cells. Potassium ferrocyanide is known to undergo a reaction of photoaquation when exposed to ultra-violet light, $Fe(CN)_6^{4-} + H_2O \rightleftarrows Fe(CN)_5H_2O^{3-} + CN^-$, resulting in an increase in solution pH due to the protonation of the cyanide ion, $CN^- + H_2O \rightleftarrows HCN + OH^-$, a process which can alter the curvature of lipid membranes[7]. Increasing pH is known to induce echinocytosis[8]. The experiments were performed in a dark room and photoaquation was initiated with light of wavelength 367 nm provided by a Till Photonics Polychrome V monochromator mounted in epi-illumination mode on an Olympus IX50 inverted microscope.

Figure S7 shows the induced discocyte-echinocyte transformation once the photochemical reaction was initiated by illuminating the cell suspension chamber with light (367 nm). The bulges around the cell equator can be clearly identified in the second image. Again, $\langle c_9 \rangle$ proved to be a reliable parameter for this transition, and its value increased approximately three-fold.

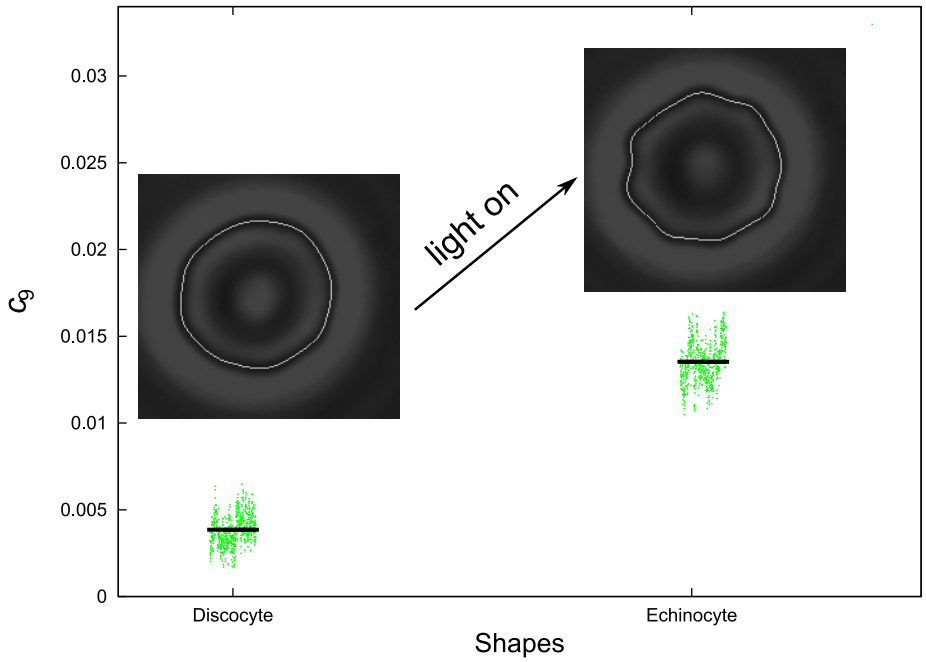

Figure S7. Changes in the 9th Fourier mode amplitude as a result of shape transitions induced by increase in pH. The points in each green cluster represent the instantaneous values of c_9. The black line across each cluster is the mean value for this amplitude, $\langle c_9 \rangle$. Representative snapshots (phase contrast) of the corresponding shapes are shown above each cluster. The white line is the reconstructed contour.

References

1. A. L. Keyburn, T. L. Bannam, R. J. Moore and J. I. Rood, *Toxins*, 2010, **2**, 1913.
2. X.-X. Yan, C. J. Porter, S. P. Hardy, D. Steer, A. I. Smith, N. S. Quinsey, V. Hughes, J. K. Cheung, A. L. Keyburn and M. Kaldhusdal, *MBio*, 2013, **4**, e00019.
3. H.-G. Döbereiner, G. Gompper, C. K. Haluska, D. M. Kroll, P. G. Petrov and K. A. Riske, *Phys. Rev. Lett.*, 2003, **91**, 048301.
4. G. Lim H. W., M. Wortis and R. Mukhopadhyay, in *Soft Matter, Vol. 4: Lipid Bilayers and Red Blood Cells*, eds. G. Gompper and M. Schick, WILEY-VCH Verlag GmbH & Co. KGaA, Weinheim, 2008, vol. 4, pp. 83-249.
5. A. Li, H. Seipelt, C. Müller, Y. Shi and G. M. Artmann, *Pharmacol Toxicol.*, 1999, **85**, 206.
6. S. Schrier, A. Zachowski and P. Devaux, *Blood*, 1992, **79**, 782.
7. P. G. Petrov, J. B. Lee and H.-G. Döbereiner, *Europhys. Lett.*, 1999, **48**, 435.
8. P. Wong, *J. Theor. Biol.*, 1999, **196**, 343.